Am J Physiol Lung Cell Mol Physiol 329: L756–L769, 2025.
First published October 29, 2025; doi:10.1152/ajplung.00078.2025

american physiological society

AMERICAN JOURNAL OF PHYSIOLOGY
LUNG CELLULAR AND MOLECULAR PHYSIOLOGY

METHODS AND RESOURCES

Use of patient-derived organoids for pleural mesothelioma 3-D modeling

Luca Volpini,[1]* Federica Monaco,[1]* Elisabetta Casalone,[2] Elton Jalis Herman,[2] Rebecca Filomena,[2] Sandra Manzotti,[1] Olga Strogovets,[1] Gianluca Moroncini,[1] Matteo Mozzicafreddo,[1] Antonella Poloni,[1] Elena Marinelli Busilacchi,[1] Francesca Gonnelli,[3] Francesca Barbisan,[4] Gaia Goteri,[3] Lina Zuccatosta,[5] Martina Bonifazi,[3] Giuseppe Matullo,[2,6] Jiri Neuzil,[7,8] Lory Santarelli,[1] Najib M. Rahman,[9,10,11] Kevin Blyth,[12,13] Marco Tomasetti,[1]* and Federico Mei[3]*

[1]Department of Clinical and Molecular Sciences, Polytechnic University of Marche, Ancona, Italy; [2]Department of Medical Sciences, University of Turin, Turin, Italy; [3]Department of Biomedical Sciences and Public Health, Polytechnic University of Marche, Ancona, Italy; [4]Department of Internal Medicine, Pathological Anatomy Unit, AOU of Marche, Ancona, Italy; [5]Interventional Pulmonology Unit, Department of Onco-Hematology and Thoracic Diseases, Azienda Ospedaliera di Rilevanza Nazionale «Antonio Cardarelli», Naples, Italy; [6]Medical Genetics Unit, AOU Città della Salute e della Scienza, Turin, Italy; [7]Laboratory of Molecular Therapy, Institute of Biotechnology, Czech Academy of Sciences, Prague-West, Czech Republic; [8]School of Pharmacy and Medical Science, Griffith University, Southport, Queensland, Australia; [9]Oxford Centre for Respiratory Medicine, Oxford University Hospitals NHS Trust, Oxford, United Kingdom; [10]Oxford Respiratory Trials Unit, University of Oxford, Oxford, United Kingdom; [11]Oxford Chinese Academy of Medicine Institute, Oxford, United Kingdom; [12]Glasgow Pleural Disease Unit, Queen Elizabeth University Hospital, Glasgow, United Kingdom; and [13]School of Cancer Sciences, University of Glasgow, Glasgow, United Kingdom

Abstract

Defining preclinical models is of utmost importance for pleural mesothelioma (PM) to improve prognosis and predict therapeutic response. Using cells isolated from pleural fluid (PF) and diagnostic pleural biopsy (PB), we generated PM patient-derived organoids (PM-PDOs) and reactive-mesothelial (RM) patient-derived organoids (RM-PDOs) aiming at assessing the proportion of successful cultures both from PF and PB. We also compared the architectural and immune-histochemical features of PM-PDOs with those of parental tissues and evaluated the PM-PDOs response to chemoimmunotherapy. We obtained 11 successful PM-PDOs from 15 PF/PB (73.3%). The rate of success was higher in epithelioid PM (88.8%) compared with biphasic PM (40.0%) ($P = 0.175$), and when using PF (60.0%) compared with PB (20.0%) ($P = 0.001$). We also obtained 3 RM effective cultures from 6 asbestos-exposed patients (50%) with nonspecific pleuritis. Transcriptome analysis identified gene expression profile in PM-PDOs, which differentiate from RM-PDOs. PM-PDOs successfully maintained the histological architecture and molecular markers of their parental tumor tissues. The macrophagic component ($CD68^+$ and $CD163^+$) was an important component in RM-PDOs and was present in all three PM histotypes. Epithelioid PM-PDOs showed resistance to both Cis/PeMtx and pembrolizumab plus peripheral blood mononuclear cells (PBMCs), whereas both biphasic and sarcomatoid subtypes were sensitive to immunotherapy. Notably, immunotherapy induced an upregulation of PD-L1 expression and activated the STAT3/NF-κB signaling pathway, suggesting a mechanism of immune evasion. PF offers a valuable source of cancer and stromal cells to generate PDO, reinforcing its clinical utility for patients who cannot undergo invasive procedures.

NEW & NOTEWORTHY Using cells isolated from pleural effusion and pleural biopsy, we established an efficient 3-D culture system for generating PM and reactive mesothelial (RM) patient-derived organoids. PM-PDOs expressed a specific gene profile, preserved the histological architecture, showing markers of the parental tumor tissues and recapitulated the tumor microenvironment (e.g., macrophages and tumor lymphocytes), which is an important factor influencing responses to therapy. This approach will be useful for drug screening, contributing to a more accurate selection of therapeutic options.

immunotherapy; patient-derived organoids; PD-L1; pleural mesothelioma; reactive mesothelial

INTRODUCTION

The burden of malignant pleural mesothelioma (PM) is significant, and the number of cases and deaths will be increasing due to aging population (1–5) and to persistent asbestos use and production worldwide despite its ban in many countries (6, 7). This neoplasm originates from hyperplasia and metaplasia of pleural mesothelial cells. The overlapping morphological features of benign reactive mesothelial (RM) lesions and PM complicate the pathological diagnosis (8). In

*L. Volpini, F. Monaco, M. Tomasetti, and F. Mei contributed equally to this work.
Correspondence: F. Gonnelli (francygonnelli@gmail.com).
Submitted 10 March 2025 / Revised 10 June 2025 / Accepted 14 October 2025

~40% of cases, the histological findings show nonspecific patterns of inflammation and fibrosis (nonspecific pleuritis, NSPs), and ~6% of them are eventually diagnosed with PM (9). Despite recent advances in systemic therapies and widespread asbestos ban, PM prognosis is still poor (10, 11). Therefore, new effective models to better understand PM behavior and, potentially, to establish tailored therapeutic pathways are highly warranted. In this context, patient-derived organoids (PDOs) may represent a valuable source for research, as they resemble the in vivo anatomy and physiology of parental organs (12), with preserved extracellular matrix and tumor microenvironment.

This aspect is particularly relevant as the cross talk between cancer and stromal cells may influence not only the tumor behavior but also therapeutic response. In fact, the interplay between the immune system, tumor suppressor genes, and immune senescence has recently been highlighted (13), laying the foundations of adoption of immune checkpoint inhibitors (ICIs) (i.e., nivolumab with or without ipilimumab) in treatment of patients with unresectable PM (14, 15). However, the response to therapy seems to be related to the histological type, as the latest RCTs and meta-analyses showed that immunotherapy may be a better choice compared with chemotherapy in nonepithelioid subtype, whereas it has not shown survival benefit in patients with epithelioid subtypes (14, 16).

Therefore, there is an ever-growing need for noninvasive or minimally invasive techniques to predict the tumor behavior and the response to chemo- and immunotherapy to accelerate drug development. Pleural fluid (PF) may represent a valuable source as it is the most common initial presentation in PM, especially in patient with the epithelioid subtype (17, 18), and comprises a wide number of cell types (i.e., immune cells and stromal cells) that accurately reflect the heterogeneity of PM cellularity (19).

In our study, we aimed at generating ex vivo 3-D cell culture models (i.e., PDOs) from PF and pleural biopsy (PB) in patients with high suspicion for PM to assess the proportion of successful cultures both in PF and in PB. As secondary aims, we compared morphological and immunohistochemical (IHC) features of PDOs with parental tissue and, finally, we evaluated the response of PM-PDOs to chemotherapy (i.e., cisplatin/pemetrexed, Cis/PeMtx) and immunotherapy (pembrolizumab + peripheral blood mononuclear cells, Pemb + PBMCs) in all histological subtypes.

MATERIALS AND METHODS

Population

Patients who underwent medical thoracoscopy or video-assisted thoracoscopy surgical for suspected thoracic cancers were recruited at the Diagnosis and Treatment of Interstitial Lung Disease, Pleural Disease and Adults Bronchiectasis Unit and Respiratory Disease Unit, Marche University Hospital, Ancona, Italy, from November 2021 to November 2023. Inclusion criteria were *1*) age > 18 yr; *2*) environmental/occupational exposure to asbestos; *3*) presence of unilateral pleural effusion; and *4*) pleural lesions/pleural thickening detected by computed tomography (CT) scan. To avoid any confounding effect due to other concomitant malignancy, we excluded all patients with a known oncologic disease other than PM or a history of radical surgery, radiotherapy, or chemotherapy in the previous 12 mo.

We collected PF and PB samples as part of standard treatment. Histological diagnosis was performed on PB. We further classified PM cases into epithelial (EPM), biphasic (BPM), and sarcomatoid (SPM).

PDO Culture

A sample of PF and, whether available, a fragment PB were collected and immediately used for organoid preparation, as follows. The PF (between 500 and 1,000 mL) was centrifuged at 1,600 rpm, and the pellet was washed twice with PBS and incubated in 10 mL of red blood cells ammonium chloride lysis buffer (8 g NH_4Cl, 0.84 g $NaHCO_3$, and 0.37 g EDTA in 100-mL water) for 20 min and resuspended in 5–10 mL PBS.

An aliquot of pellet was used for peripheral blood mononuclear cells (PBMCs) isolation. Briefly, 6 mL of the suspension was layered onto 4 mL Lympholyte-H (Cederlane, Hornby, ON, Canada) and centrifuged at 700 *g* (20°C, 30 min). After centrifugation, the cloudy layer was collected and washed in PBS, and the pellet resuspended in freezing medium was cryopreserved.

The PB (between 5 and 10 mg) was mechanically disrupted to 5–6 pieces of 1 mm^3 tissue and enzymatically digested in advanced DMEM/F12 (adDMEM/F12; Gibco, Thermo Fisher, MA) supplemented with 2% FBS and collagenase/hyaluronidase (1 mg/mL), at 37°C for 15–30 min with intermittent stirring. After incubation, the suspension was disrupted by repeated pipetting and passing through a 100-µm cell strainer (BD Falcon, CA). After enzyme inhibition with 10% FBS, the slurry was centrifuged at 1,600 rpm for 5 min at RT and the pellet washed in PBS and resuspended in 0.5–1 mL PBS.

Cell density was evaluated using the Burker chamber. Cell suspension corresponding to 70%–80% cell confluency was centrifuged at 1,600 rpm for 5 min at RT and resuspended in the same volume of ice-cold Reduced Growth Factor Basement Membrane Matrix (Matrigel; Corning, No. 356234, NY) or Hydrogel (Photocol-IRG, Methacrylated Collagen Hydrogel, No. CC320; Merck, Darmstadt, Germany). PF and PB samples were collected from each patient, and the obtained cell suspension was encapsulated in both Matrigel and Hydrogel matrix for organoid formation according to the scheme shown in Fig. 1. Drops of 30–40 µL of both basement membrane extracellular matrix were placed into wells of a 24-well plate, kept on ice, and after solidification in the CO_2 incubator at 37°C, 400 µL of optimized PDO medium was added to the wells. Several culture media have been proposed for PDO culture, with their composition varying depending on the tissue type and sample source (20–23). We tested three media for PDO preparation and growth: a complete medium elective for mesothelioma cell culture and a medium proposed for PDO culture with and without stemness supplements. Therefore, RPMI-1640 with 10% FBS and 1% penicillin/streptomycin (PDO medium-1); AdDMEM/F12 containing, 2 mM GlutaMAX, 1% penicillin/streptomycin, 2 mM HEPES (AdDF +++) plus 20 ng/mL EGF, 20 ng/mL FGF2, 10 µM Y-27632, and B27 and N2 supplements (PDO medium-2); and AdDF +++ plus 20 ng/mL EGF, 20 ng/mL

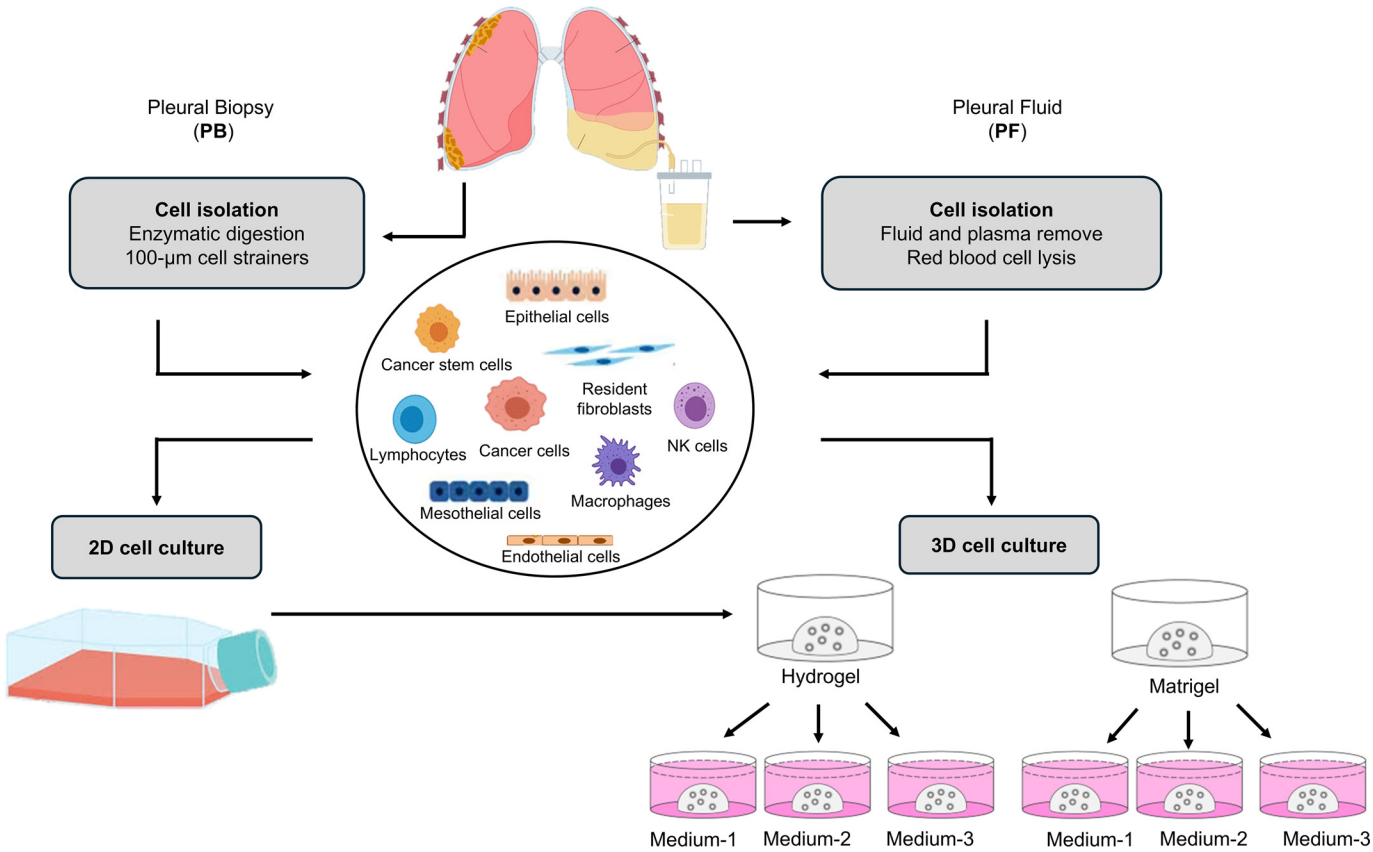

Figure 1. Flowchart of sample collection and three-dimensional cell culture formation. NK cells, natural killer cells.

FGF2, and 10 μM Y-27632 (PDO medium-3) were used (Supplemental Table S1). Organoids were cultured over 1 mo with changing fresh medium every 4 days.

Morphology and IHC

As PDOs should reproduce primary tumor key features, we performed hematoxylin and eosin (H&E) staining and immunohistochemistry (IHC) analysis to assess whether viable organoids maintained characteristics parental organ. Tissues and organoids were fixed in 4% formaldehyde followed by dehydration, paraffin embedding, sectioning, and standard hematoxylin and eosin (H&E) staining. Immunohistochemistry (IHC) was performed in formalin-fixed, paraffin-embedded tumor sections (2.5 μm) by incubation with primary antibodies including anti-epithelial-related antigen (AE1/AE3), anti-podoplanin (D2-40), anti-calretinin (CAL), anti-cytokeratin 5/6 (CK5/6), anti-Wilms' tumor 1 protein (WT1), anti-α-smooth muscle actin (α-SMA), anti-CD31, anti-vimentin, anti-CD68, anti-CD163, anti-CD3, anti-CD8, anti-BRCA1-associated protein 1 (BAP-1), and anti-PD-L1, all from Dako, CA. The anti-STAT3, anti-pSTAT3, anti-AKT, anti-pAKT, anti-NF-kB-p65, all from Cell Signaling (Cell Signaling Technology, Danvers, MA). The sections were subsequently incubated with secondary antibodies (Dako, CA) and visualized using the ultraView Universal DAB Detection kit (Dako, CA). Nuclei were counterstained with hematoxylin. Images were acquired with an optical microscope (Zeiss, Axiocam MRc5; magnification ×20). All sections and staining were assessed by an expert malignant mesothelioma pathologist (F.B.).

Transcriptome Analysis

Total RNA was extracted from PM-PDOs of epithelial subtype and reactive mesothelial organoids (RM-PDOs, $n = 3$) using miRNeasy Micro Kit (Qiagen, Hilden, Germany). RNA integrity number (RIN value) was assessed using the Agilent 2100 Bioanalyzer with the RNA 6000 Nano kit (Agilent Technologies, California) and RNA concentration using the RNA HS assay in Qubit 4.0 (Life Technologies, Thermo Fisher, Massachusetts). RNA libraries were prepared using KAPA RNA HyperPrep Kit with RiboErase (HMR) (Roche Molecular Systems, Switzerland). The quality and concentration of the libraries were assessed using the DNA high sensitivity kit in the 2100 Bioanalyzer Instrument (Agilent Technologies, California) and Qubit Fluorometric Quantification (Qubit dsDNA HS assay; Life Technologies, Thermo Fisher, Massachusetts), respectively. Paired-end RNA-seq (2 × 75 bp) was done with the Illumina NextSeq550 sequencing instrument (Illumina, California). Read pairs were mapped and quantified to the human GRCh38 reference genome using the Salmon tool (24). The generated counts were extracted with DESeqDataSetFromTximport function, and gene level differential expression analysis was performed using Deseq2 R package, estimation of fold change, and dispersion for RNA-Seq data with DESeq2 (25). *P* values were adjusted for gender and age to control the global false discovery rate (FDR). Heatmaps were generated using the heatmap2 package (Kolde R Pheatmap: pretty heatmaps R Package v. 2012); PCA and volcano plots were prepared using the ggplot2 package (26).

To perform KEGG pathway and gene ontology (GO) analysis, a log-transformed normalized count-permillion matrix was derived using the R package. To cluster and visualize the enriched terms, we used the PathFindR (v. 2.5.1).

Lymphocyte Phenotypic Analysis

PBMCs isolated from PF and whole blood of patients with PM were checked for their viability by 7AAD-PerCP staining and then incubated with labeled primary antibody against CD3-FITC, CD4-PE-Cy7, CD8-APC, CD19-APC-Cy7, CD25-APC-R700, CD8-V450, CD45-V500, and CD56-PE, all from Becton Dickinson. Fluorescence emission was detected by flow cytometry (FACS Lyric; Becton Dickinson), and the lymphocyte subpopulations were expressed as percentage over total population.

Drug Treatment

We evaluated the response to cisplatin (cis)-pemetrexed (PeMtx) and ICI-anti-PD-1 (pembrolizumab) (27). An in vitro immunotherapy model was established by treating the PDOs with the pembrolizumab in the presence of PBMCs isolated from the same patient. Given the crucial role of immunological cells in the immunotherapy-induced tumor suppression, we also characterized the cellular components of PF: PBMC subpopulations expressing different antigens were identified and compared with PBMC obtained from whole blood (WB). PM-PDOs were treated in triplicate with cisplatin/pemetrexed (Cis/PeMtx, 30 μM each), or with pembrolizumab (Pemb, 10 μg/mL) in coculture with PBMCs (10^5) obtained from the same patient. Untreated PM-PDOs were used as negative control. We applied two cycles of treatment with a 3-day interval between cycles. Treated and nontreated PM-PDO controls were collected 3 days after the last treatment cycle, then fixed in formalin, and evaluated for tissue markers (AE1/AE3, D2-40, vimentin) macrophages (CD68 and CD163), T-cells (CD3 and CD8), and STAT3, PD-L1, AKT, and NF-kB-p65 by IHC analysis. PM-PDOs were inspected using an optical microscope (Zeiss, Axiocam MRc5; magnification ×2.5 and ×10), and the effect of treatment was blinded and evaluated at the same time and conditions and expressed as the number, size (μm), and optical intensity of organoids using ImageJ.

Statistical Analysis

Continuous quantitative variables are presented as means ± standard deviation (SD). We calculated the proportion of successful PDOs. We compared the proportion of successful cultures when using PF versus PB and those of EPM versus BPM using the Fisher exact test.

We used the Mann–Whitney *U* test, two-tailed Student's *t* test, and one-way ANOVA analysis of variance with Tukey's post-hoc to calculate the differences in terms of PDO number and optical intensity between pre- (T0) and post- (T1) among treatments both for EPM-PDOs and BPM-PDOs. Probability values < 0.05 were considered significant. Statistical analyses were performed using the SPSS statistical package (SPPS, Chicago, IL).

RESULTS

Study Population

We included 15 patients with PM with a mean age of 81 ± 6 yr and a male predominance (60.0%). Nine of them (60.0%) were diagnosed with epithelioid subtype, 5 (33.3%) with biphasic subtype, and 1 with sarcomatoid subtype (Table 1).

We also included 6 patients diagnosed with nonspecific pleuritis (NSP). Five of them were male (83.3%), and they had a mean age of 80 ± 4 yr (Table 1). The demographic, pathological characteristics, and PDO formation of enrolled population are shown in Supplemental Table S2.

Malignant Pleural Mesothelioma-PDOs

Among the 15 PM, we were able to generate 11 successful PDOs (73.3%). We obtained 9 PDOs from PF (81.8%), 2 PDOs (18.2%) from PB only, and 1/11 (9%) PDOs from both PF and PB, with a proportion of 66.7% (10/15) in case of PF and 20.0% (3/15) when using PB ($P = 0.001$). The proportion of successful cultures was 88.9% in epithelioid PM (8/9), 40.0% in biphasic PM (2/5), and 100% sarcomatoid (1/1) ($P = 0.175$) (Table 1).

Notably, Matrigel resulted the best EMB to ensure PM-PDOs and grew better in PDO medium-1 and PDO medium-3, whereas the addition of stemness supplements (PDO medium-2) often reduced organoid development and growth (Supplemental Fig. S1 and Supplemental Table S3).

Reactive Mesothelial-PDOs

We obtained 3/6 (50%) reactive mesothelial PDOs (RM-PDOs). Overall, RM-PDOs were produced from PF with a successful rate comparable with the PM-PDO one (Table 1). In all three NSP patients (100%) where PDOs were acquired, a benign evolution was eventually confirmed after 1-year follow-up.

Table 1. *Demographic and clinical features and rate of PDO generation of our study population*

PM ($n = 15$)	
Age, yr (± SD)	81 ± 6
Gender (Male), *n* (%)	9/15 (60.0%)
PM Histotype	
EPM, *n* (%)	9/15 (60.0%)
BPM, *n* (%)	5/15 (33.3%)
SPM, *n* (%)	1/15 (6.7%)
Rate of PM-PDO generation, *n* (%)	11/15 (73.3%)
Epithelioid	8/9 (88.9%)
Biphasic	2/5 (40.0%)
Sarcomatoid	1/1 (100%)
Source	
PF	10/15 (66.7.0%)
PB	3/15 (20.0%)
RM ($n = 6$)	
Age, yr (± SD)	80 ± 4
Gender (Male), *n* (%)	5/6 (83.3%)
Rate of RM-PDO generation, *n* (%)	3/6 (50%)
Source	
PF	3/6 (50.0%)
PB	0/6 (0.0%)

B, biphasic; E, epithelioid; PB, pleural biopsy; PDO, patients-derived organoids; PF, pleural fluid; PM, pleural mesothelioma; RM, reactive mesothelial; S, sarcomatoid.

Morphologic and IHC Features of PDOs

PM-PDOs.

Epithelial PM-PDOs. EPM-PDO, obtained from both PF and PB, grew as spheroidal mass with or without linking spindle cells and/or as network-like structures connecting neoplastic nodules (Fig. 2, *A* and *B*). This aspect adequately mimicked parental tissues including multifocal growth and reflected the subtype characteristics.

H&E staining revealed aligned stromal cells and clusters of cancer cells with stromal components.

We found that EPM-PDOs displayed malignant features with positivity of PM markers (i.e., AE1/AE3, D2-40, CK5/6, WT1, and vimentin), as observed in parental tumor tissue (Fig. 2*C*). Fibroblasts (α-SMA) and endothelial cells (CD31) were not detected. The presence of $CD68^+$ and $CD163^+$ macrophages was observed both in the parental tumor tissue and at the edges of PM-PDOs.

Biphasic PM-PDOs.

BPM-PDOs, obtained from both PF and PB, showed positivity for markers of PM, such as AE1/AE3 and D2-40, as observed also in the parental tumor tissue (Fig. 3, *A*–*C*). Fibroblasts were present in the stroma, whereas the presence of $CD68^+$ cells was not detected (Fig. 3*B*). Differently, the absence of fibroblasts and presence of macrophages $CD68^+$ cells were found in BPM-PDO from PF (Fig. 3*D*).

Sarcomatoid PM-PDOs.

SPM-PDOs, obtained from PB, growth as spheroidal mass. The organoids morphologically mimicked parental tissue and adequately recapitulated the subtype characteristics. IHC analysis showed that SPM-PDOs displayed malignant features with positivity of PM markers, such as AE1/AE3, D2-40, CK5/6, CAL, and WT1 and negativity to BAP-1, as observed in the parental tumor tissue. No presence of fibroblasts (α-SMA) was found, whereas positivity for $CD68^+$ macrophages was observed both in PDO and parental tumor tissue (Fig. 4).

Furthermore, we compared the positivity to PM markers in PDOs with those of parental tumor tissues, finding a concordance in 90% (9/10) for AE1/AE2, 100% (10/10) for D2-40, 50% (5/10) for CK5/6, 0% (0/10) for CAL, 90% (9/10) for WT1, 80% (8/10) for BAP1, and 90% (9/10) for CD68 (Table 2).

Reactive mesothelial-PDOs and transcriptome analysis. RM-PDOs developed as multifocal masses growing

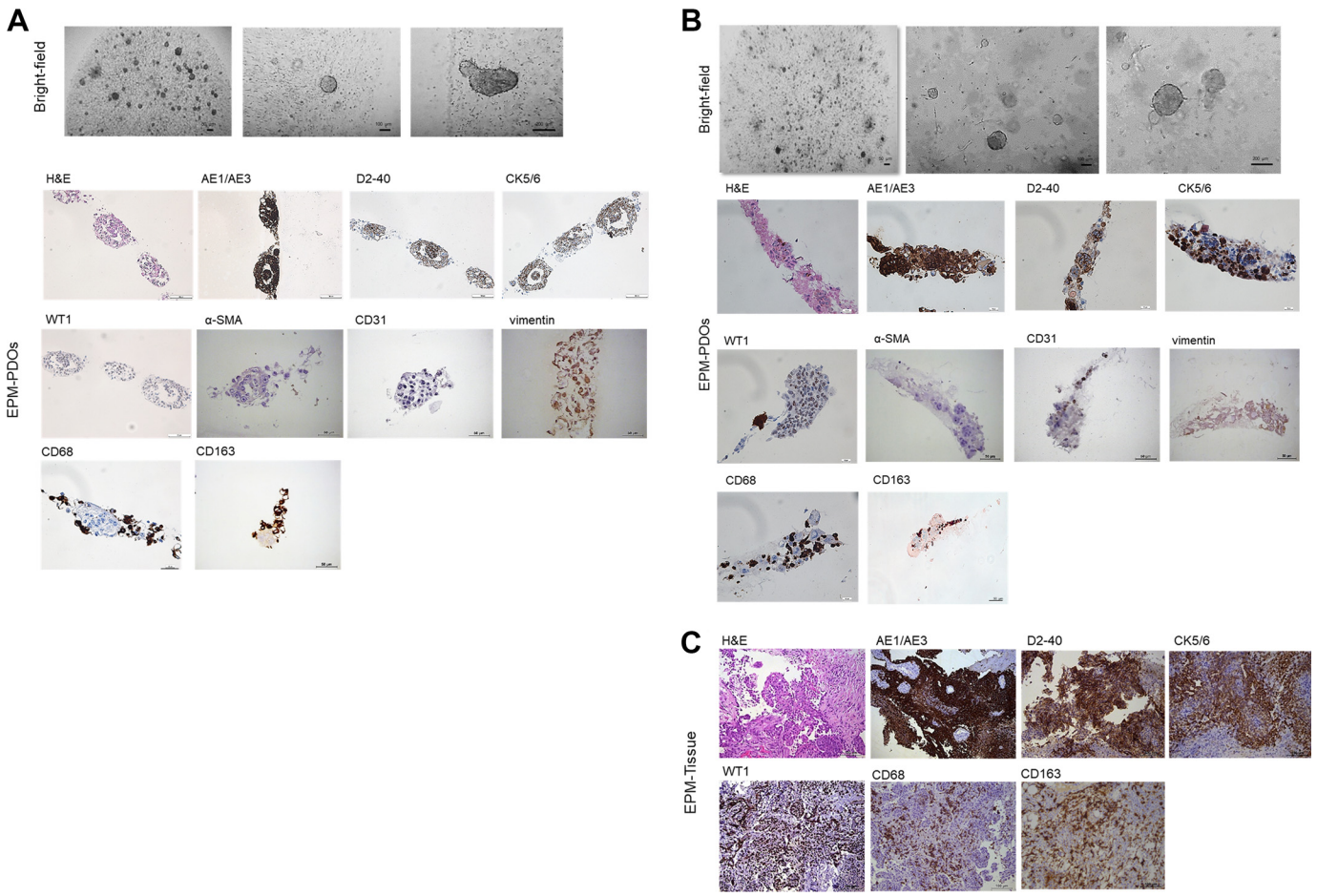

Figure 2. Epithelial malignant pleural mesothelioma patient-derived organoids (EPM-PDOs) from pleural fluid (PL) (*A*) and from pleural biopsy (PB) (*B*). Representative bright-field microscopy images (scale bar, 50 μm, 100 μm, and 200 μm). Histological assessment using H&E and IHC staining of epithelial-related antigen (AE1/AE3), podoplanin (D2-40), cytokeratin 5/6 (CK5/6), Wilms' tumor 1 protein (WT1), α-smooth muscle actin (α-SMA), CD31, vimentin, CD68, and CD163 in organoids (scale bar, 50 μm), and (*C*) parental PM tissue (scale bar, 100 μm). H&E, hematoxylin and eosin; IHC, immunohistochemical; PM, pleural mesothelioma.

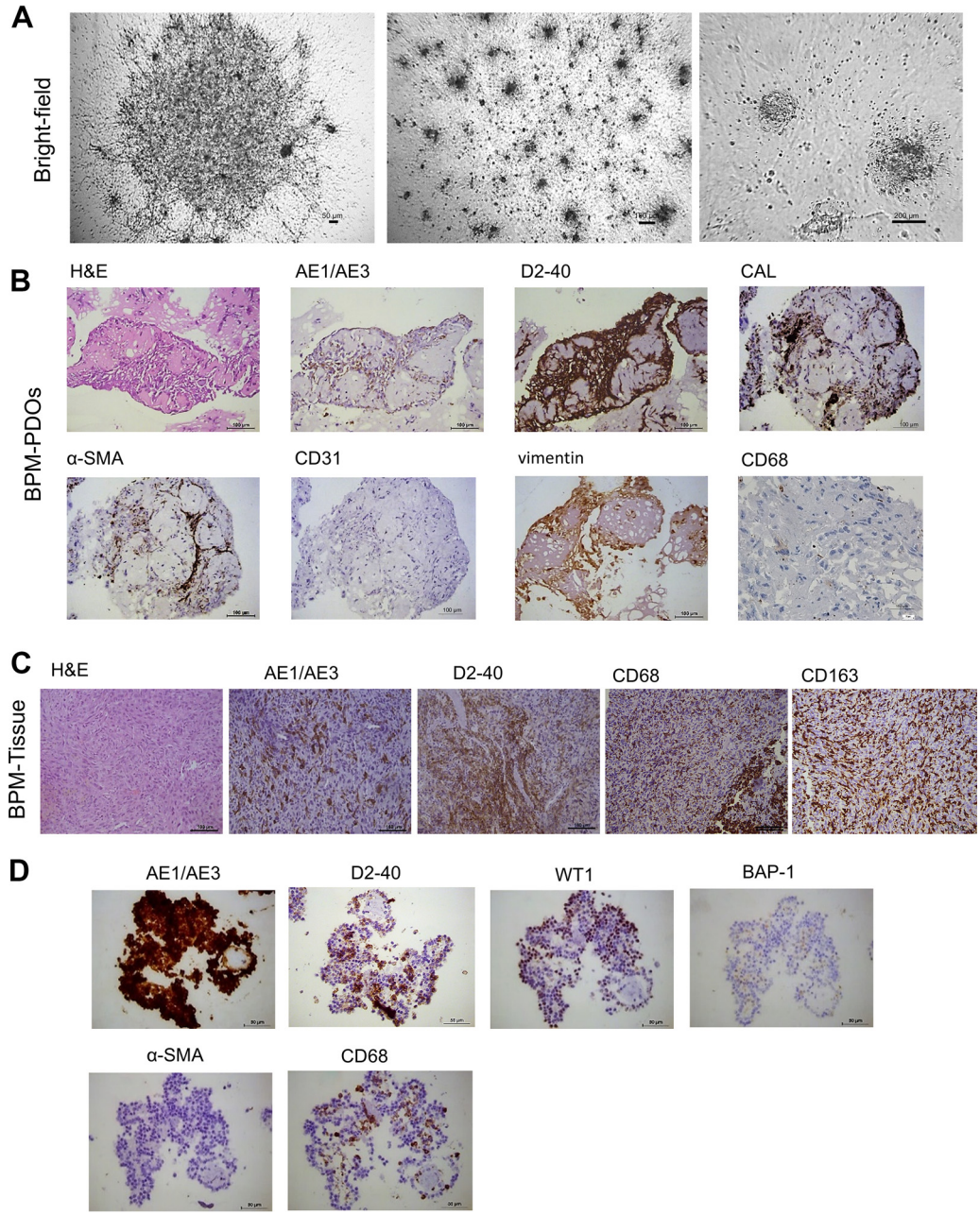

Figure 3. Biphasic malignant pleural mesothelioma patient-derived organoids (BPM-PDOs). *A*: representative bright-field microscopy images (scale bar, 50 µm, 100 µm, and 200 µm). *B*: histological assessment by H&E and IHC staining of epithelial-related antigen (AE1/AE3), podoplanin (D2-40), calretinin (CAL), α-smooth muscle actin (α-SMA), CD31, vimentin, CD68, and CD163 in organoids from PB and parental PM tissue (*C*). *D*: histological assessment by IHC staining of epithelial-related antigen (AE1/AE3), podoplanin (D2-40), Wilms' tumor 1 (WT1), BAP-1, α-smooth muscle actin (α-SMA), and CD68 in PDOs from PF. Scale bar, 50 µm. H&E, hematoxylin and eosin; IHC, immunohistochemical; PM, pleural mesothelioma.

intermingled with stromal cells. RM-PDOs were positive both to epithelial-related antigen (i.e., AE1/AE3) and to mesothelial markers (i.e., D2-40). $CD68^+$ cells were highly represented (Fig. 5). The comparison between RM-PDOs and PM-PDOs transcriptomes showed 699 significantly differentially expressed genes (P-FDR < 0.05, Fig. 6*A*). Among these, 629 genes were downregulated and 70 were upregulated in PM-PDOs compared with RM-PDOs. Heatmap depicting the differentially expressed genes shows a distinct difference in gene expression pattern in malignant and nonmalignant PDOs (Fig. 6*B*). Venn diagram indicates that PM and RM share 545 genes (78.0%), whereas 145 genes are RM-specific (20.7%) and 9 genes are PM-specific (1.3%) (Fig. 6*C*). The overall clustering is further illustrated by PCA, highlighting differences between malignant mesothelioma and reactive mesothelium (Fig. 6*D*). The KEGG analysis showed that down-expressed genes in PM-PDOs were involved in ATP-dependent chromatin modeling, including oxidative phosphorylation and chemical carcinogenesis. By analyzing the GO data, we found that innate immune response, chromatin remodeling and ERK1/ERK2 pathway were the PM-specific downregulated biological

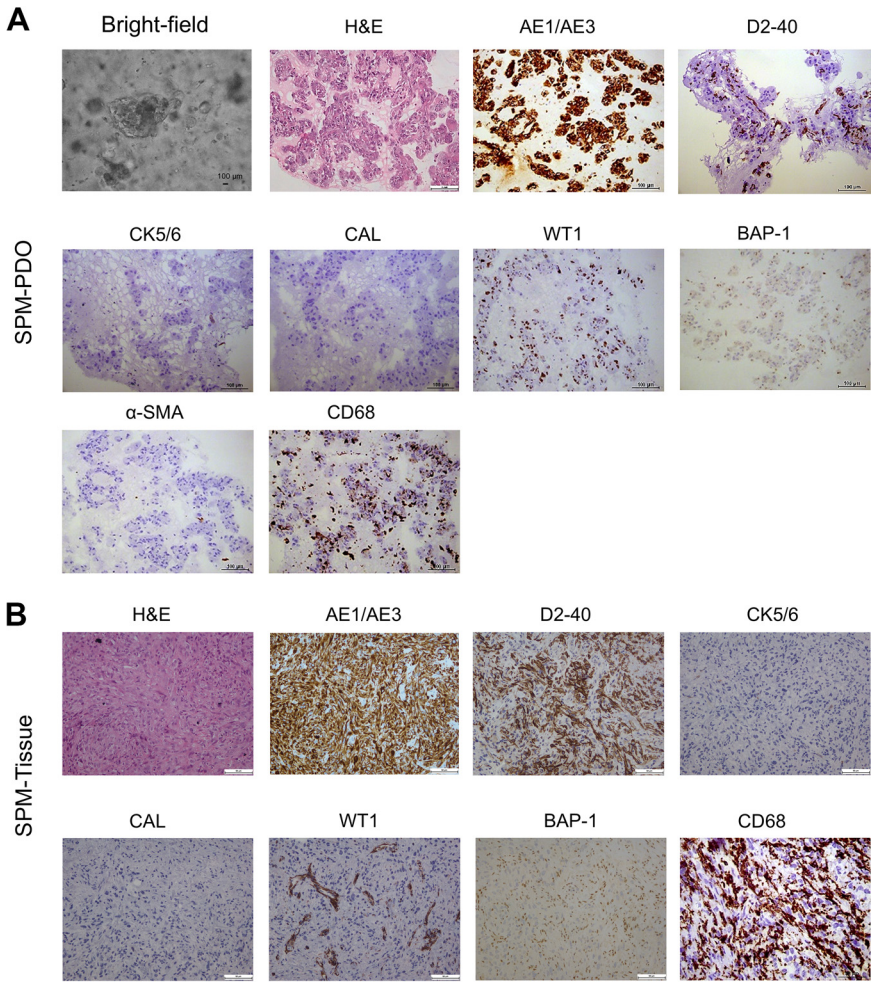

Figure 4. Sarcomatoid malignant pleural mesothelioma patient-derived organoids (SPM-PDOs). Representative bright-field microscopy images and histological assessment by H&E and IHC staining of epithelial-related antigen (AE1/AE3), podoplanin (D2-40), cytokeratin 5/6 (CK5/6) (*A*) calretinin (CAL), Wilms' tumor 1 protein (WT1), BAP-1, a-smooth muscle actin (α-SMA), and CD68 in organoids (*B*) from PB and parental PM tissue. Scale bar, 50 µm and 100 µm. H&E, hematoxylin and eosin; IHC, immunohistochemical; PB, pleural biopsy; PM, pleural mesothelioma.

process, where chromatin was the downregulated cellular components (Supplemental Fig. S2).

RESPONSE TO CHEMOIMMUNOTHERAPY. PF mainly consisted of inflammatory CD45$^+$ cells (94.8%), represented for 72% of lymphocytes T and 13% of macrophages (Supplemental Fig. S3). The immunophenotype analysis of PBMCs isolated from PF and from WB showed comparable cellular composition, except for TNK cells, which were higher in circulating PBMCs. Notably, within the T cell population, the PF showed higher helper T cells and activated T cells when compared with T cell population from WB (Supplemental Fig. S4).

No sign of cell death or reduced organoid size were found in EPM-PDOs (PM-6) after Cis-PeMtx-chemotherapy or immunotherapy (Fig. 7*A*, *right*). The IHC showed that the therapy did not affect either mesothelioma cancer cells or macrophages (Fig. 7*B*). The presence of CD68$^+$ and CD163$^+$ cells was observed within the stroma both before and after treatments. In addition, the presence of CD3 and CD8 positive cells within the PDO stroma confirmed the reliability of the immunotherapy model (Fig. 7*C*). Increased expression of PD-L1 was associated with the activation of the STAT3/NF-κB pathway in EPM-PDOs cocultured with PBMCs after pembrolizumab treatment (Fig. 7*D*).

The lack of response to chemoimmunotherapy observed in PM-PDOs of epithelial subtype (PM-13), paralleled the clinic response of the patient. The patient received two

Table 2. *Pleural mesothelioma markers in PDOs and parental tissues*

	EPM-1		EPM-2		BPM-3		EPM-6		EPM-8		EPM-10		EPM-11		EPM-13		BPM-14		SPM-15	
	PT	PDO	PT	PDO	PT	PDO	PT	PDO	PT	PDO	PT	PDO	PT	PDO	PT	PDO	PT	PDO	PT	PDO
AE1/AE3	+	−	+	+	+	+	+	+	+	+	+	+	+	+	+	+	+	+	+	+
D2-40	+	+	+	+	+	+	+	+	+	+	+	+	+	+	+	+	+	+	+	+
CK5/6	+	−	+	+	−	−	+	−	+	−	+	+/−	+	−	+	+	+	+	+	−
CAL	+	−	+	−	−	+	+	−	+	−	+	−	+	−	+	−	+	−	+	−
WT1	+	−	+	+	−	−	+	+/−	+	+	+	+	+	+	+	+	+	+	+	+
BAP1	+	+	+	−	−	−	−	−	−	+	+	+	−	−	−	−/+	−	−	−	−
CD68	+	+	+	+	+	−	+	+	+	+	+	+	+	+	+	+	+	+	+	+

B, biphasic; E, epithelioid; PDO, patient-derived organoids; PM, pleural mesothelioma; PT, parental tissue; S, sarcomatoid.

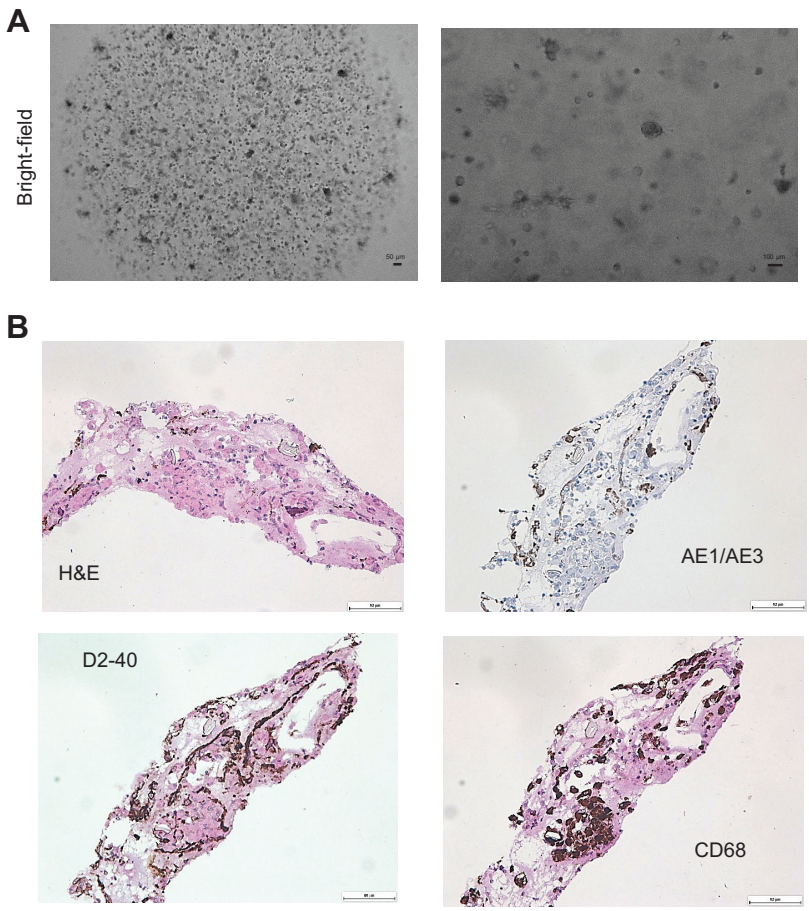

Figure 5. Histological assessment in RM-PDOs. Representative bright-field microscopy images (scale bar, 50 µm and 100 µm) (*A*) and H&E and IHC staining of epithelial-related antigen (AE1/AE3), podoplanin (D2-40), and CD68 in organoids (*B*) (scale bar, 50 µm). H&E, hematoxylin and eosin; IHC, immunohistochemical; RM-PDO, reactive-mesothelial patient-derived organoids.

cycles of carboplatin/pemetrexed chemotherapy, resulting in no response.

Conversely, a reduction in the organoid number and size was found in BPM-PDO (PM-3) cocultured with PBMCs treated with pembrolizumab (Fig. 8*A*, *right*). However, even BPM-PDO was viable and still positive for PM markers, suggesting acquisition of resistance to chemotherapy combined with immunotherapy (Fig. 8*B*). The PDOs were lacking stromal macrophages, whereas the presence of $CD3^+/CD8^+$ cells was observed in PDOs treated with pembrolizumab (Fig. 8*C*). The therapy suppressed PD-L1 expression, which was associated with reduced STAT3/NF-κB-p65 expression (Fig. 8*D*).

Sensitivity to immunotherapy was observed in PM-PDOs of biphasic subtype (PM-14) even in the presence of macrophages ($CD68^+$ cells). In this patient, stable disease was observed after nivolumab/ipilimumab before disease progression 3 mo later. Due to disease progression and side effects, the patient received carboplatin as second-line treatment.

The sarcomatoid subtype (PM-15) were significantly more sensitive to Pembrolizumab plus PBMCs treatment respect to Cis/PeMtx (Fig. 9*A*, *right*). The chemoimmune treatments do not affect the marker staining as result of drug resistance. Stromal M1-macrophages ($CD68^+$), M2-macrophages ($CD163^+$), and T-lymphocytes ($CD3^+$ and $CD8^+$) were found in PDOs (Fig. 9, *B* and *C*), which may modulate the therapeutic response by suppressing STAT3 and PD-L1 (Fig. 9*D*).

The in vitro immunotherapy response was in line with the clinical response of patient. Patient received Nivolumab/ipilimumab treatment resulting in stable disease.

DISCUSSION

In our single-center study, we confirmed the feasibility to generate PM-PDOs from PF and PB. The rate of success of PM-PDO was overall good, especially in the presence of epithelioid histotype. We were also able to create PDOs from RM in patients with a clinical and pathological diagnosis of NSP, with a good proportion of generation (50%). We also found that PF was a better source for PDO generation compared with PB, for both malignant and inflammatory pleural diseases. The EPM-PDOs and BPM-PDO were both obtained from PF and BP, whereas the only case of SPM grew from PB, but not from PF. This might be related to different growth patterns of the histotypes, as the epithelial histotype grow within the pleural surface, whereas the sarcomatoid component tends to have a more infiltrative development. This may finally influence the different trend to release cancer cells in the PF, which is higher in EPM and lower in SPM (20).

We also confirmed that the PDOs morphological and IHC features faithfully replicated those of the parental tissue, as both morphology and IHC markers were precisely overlapping. Notably, EPM-PDOs from PF and PB showed the similar stromal cellular composition, which reflect the parental tissue.

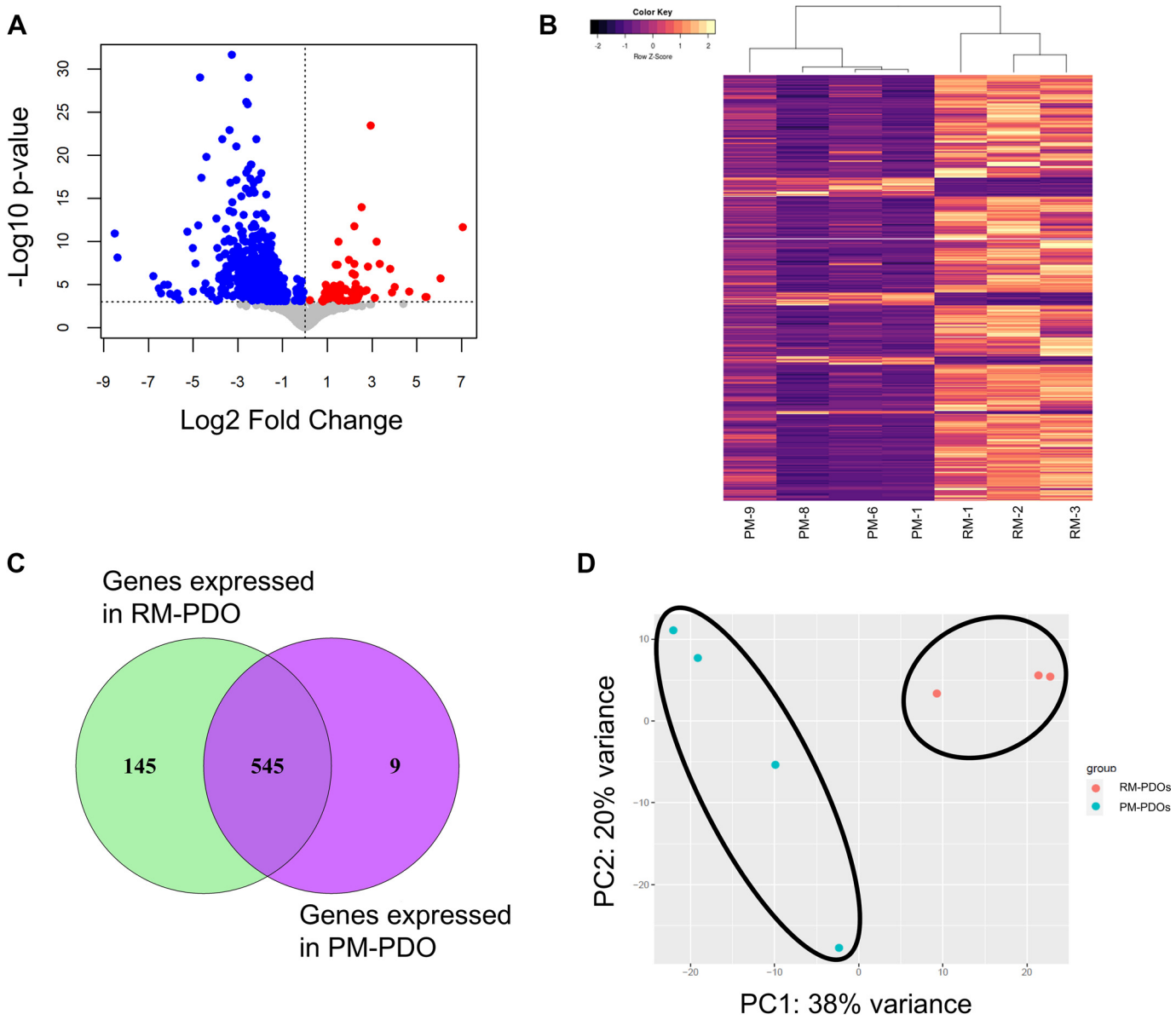

Figure 6. Transcriptomic analysis of gene expression profile of RM-PDOs and PM-PDOs. Volcano plot (*A*) and heatmap (*B*) of differentially expressed genes in the transcriptome. *C*: Venn diagram showing the number of genes specific for each PDO group. *D*: the PCA highlighting differences between malignant and reactive mesothelioma. RM-PDOs $n = 3$ and PM-PDOs $n = 3$. PM-PDOs, PM patient-derived organoids; PM, pleural mesothelioma; RM-PDO, reactive-mesothelial patient-derived organoids.

Another interesting result came from transcriptome analysis, performed to explore potential differences and similarities of gene expression in PM-PDOs and RM-PDOs. Differentially expressed genes were detected in PM-PDOs, identifying deregulated pathways such as activation of innate immune response and chromatin remodeling. Both pathways are regulated by BAP1, which is a tumor suppressor gene often associated with PM development (28, 29).

High rate of success with PF as a source for generating PDOs was previously reported by Hocking et al. (30), who established mesothelioma PDOs from PF with proportion of 50% (21–26, 28–30). In addition, Cioce et al. (31) confirmed that PF-derived PDOs reproduce the genetic characteristics of the tumor, emphasizing its utility in precision medicine (22). This underscores PF as an accessible and effective source of cancer cells for PDO generation, offering a less invasive way to get PDOs, ensuring the tumor's representativeness. However, our successful rate in establishing PM-DPOs was higher than previously reported. One of the possible explanations is the type of scaffold used for the generation of organoids. The choice of scaffold may also influence also molecule and growth factor diffusion, including chemotherapy agents and cytokines. The scaffolds used for the PDO generation may therefore bias cancer drug assays. Matrigel was the optimal basement membrane matrix to promote PM-PDO growth. In comparison with hydrogel, Matrigel contains integrin-binding peptide motives on type IV collagen and laminin-111, which is an essential process for PDO development (32). Matrigel-based MM organoids were also generated using mouse and canine PM models (33, 34).

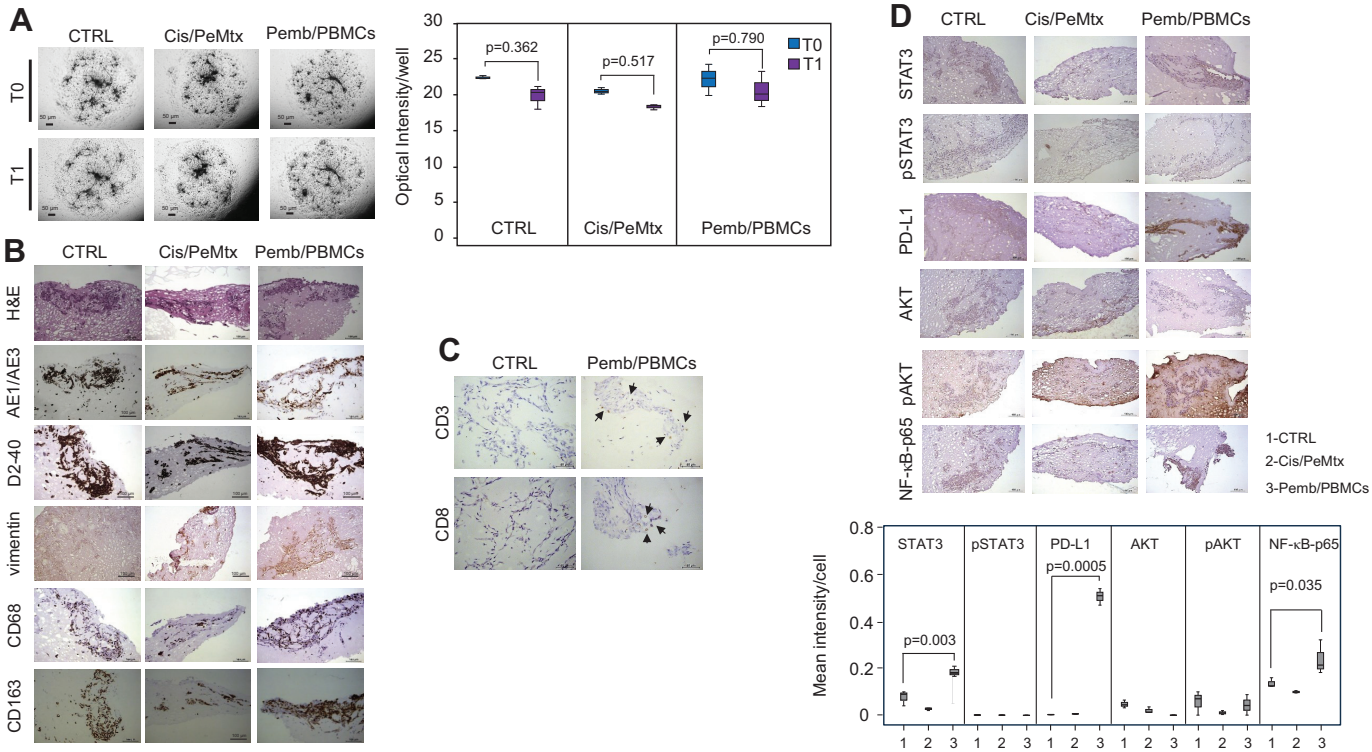

Figure 7. Drug response in EPM-PDOs. Female EPM-PDOs (PM-2) were treated with Cis/PeMtx (30 μM each) or with pembrolizumab (10 μg/mL) in coculture with PBMCs (10^5) from the same patient (Pemb/PBMCs); 2 cycles of treatments with 3 days between cycles were applied. *A*: representative bright-field microscopy images (scale bar, 50 μm). Organoid growth was quantified by optical intensity (*right*). *B*: FFPE tumor sections were inspected for H&E and immunohistochemical staining of epithelial-related antigen (AE1/AE3), podoplanin (D2-40), vimentin, CD68, and CD163. Scale bar, 100 μm. *C*: FFPE tumor sections were inspected for immunohistochemical staining of CD3 and CD8 antigen. Scale bar, 50 μm. *D*: evaluation of the PD-L1 and the STAT3/AKT/NF-κB pathway. Scale bar, 100 μm. Images for control and treatment groups in microscopy experiments were collected at the same time under the same conditions. Data shown are means ± SD of three independent experiments. Comparison between and among groups were evaluated by *t* test analysis and by 1-way ANOVA with Tukey's post hoc analysis, respectively. Cis/PeMtx, cisplatin/pemetrexed; EPM-PDOs, epithelial patient-derived organoids; FFPE, formalin-fixed, paraffin-embedded; H&E, hematoxylin and eosin; PBMCs, peripheral blood mononuclear cells; Pemb, pembrolizumab; PM, pleural mesothelioma.

Stemness supplements and growth factors such as EGF, Noggin, and R-spondin1 are widely accepted as most essential factors in the organoid medium (33, 34). In our model, we found that the N2 and B27 stemness supplements reduced growth of PDOs, thus supporting previous results showing that stemness was not required to maintain organoid growth (33). Among the three media tested, the RPMI-1640 supplemented with FBS was the optimal culture medium for PM-PDO. Using complete RPMI-1640 medium, cell components of tumor stroma growth within the organoid, thus generating a tumor microenvironment (TME) that is associated with tumor heterogenicity provided by PF as source of cells, better capture tumor features. For the first time, we established PM-PDOs with stromal cells such as macrophages that overcome one of the major limits of organoid model, which is represented by the lack of reliable immune TME. In fact, tumors also consist of a diverse nontransformed component, including fibroblasts, stromal cells, endothelial cells, and immune cells, including T cells ($CD4^+$ T-helper cells, $CD8^+$ cytotoxic T cells, and regulatory T cells), B cells, tumor-associated macrophages, and dendritic cells. TME is a complex and dynamic ecosystem that influences tumor progression, metastatic dissemination, and tumor response to therapy (35). Therefore, many studies focused on the development of a PDO-immune cell coculture model that effectively predict the patient responses to various therapies (36). Cattaneo et al. generated a functional tumor-reactive T cells based on the coculture of tumor organoids with PBMCs, showing a high level of tumor-reactive $CD8^+$ T cell populations (37).

Consistent with this, local PBMCs may constitute a distinct subpopulation—being immune-experienced and expressing different antigens—compared with circulating PBMCs and could provide a reliable immune microenvironment for testing immunotherapy at the individual level.

When testing the response to chemoimmunotherapy, we found a partial response in BPM-PDOs and SPM-PDOs, whereas a complete lack of response in EPM-PDOs. Cis-PeMtx chemotherapy did not induce PDO cell death, whereas PDOs with the sarcomatoid component were sensitive to anti-PD1 (pembrolizumab) treatment in the presence of PBMCs. These results confirm the clinical response of patients, where only patients with PM of biphasic and sarcomatoid subtype showed benefit from immunotherapy. Furthermore, we detected that immune treatment activated the NF-κB signaling pathway in PM-PDOs via the PD-1/PD-L1 axis in the presence of CD3/CD8 positive cells and macrophages. In line with this, we found that $CD68^+$ and $CD163^+$ macrophages represented an important component in RM-PDOs and were present in all PM histotypes. However, both BPM-PDOs and SPM-PDOs positively

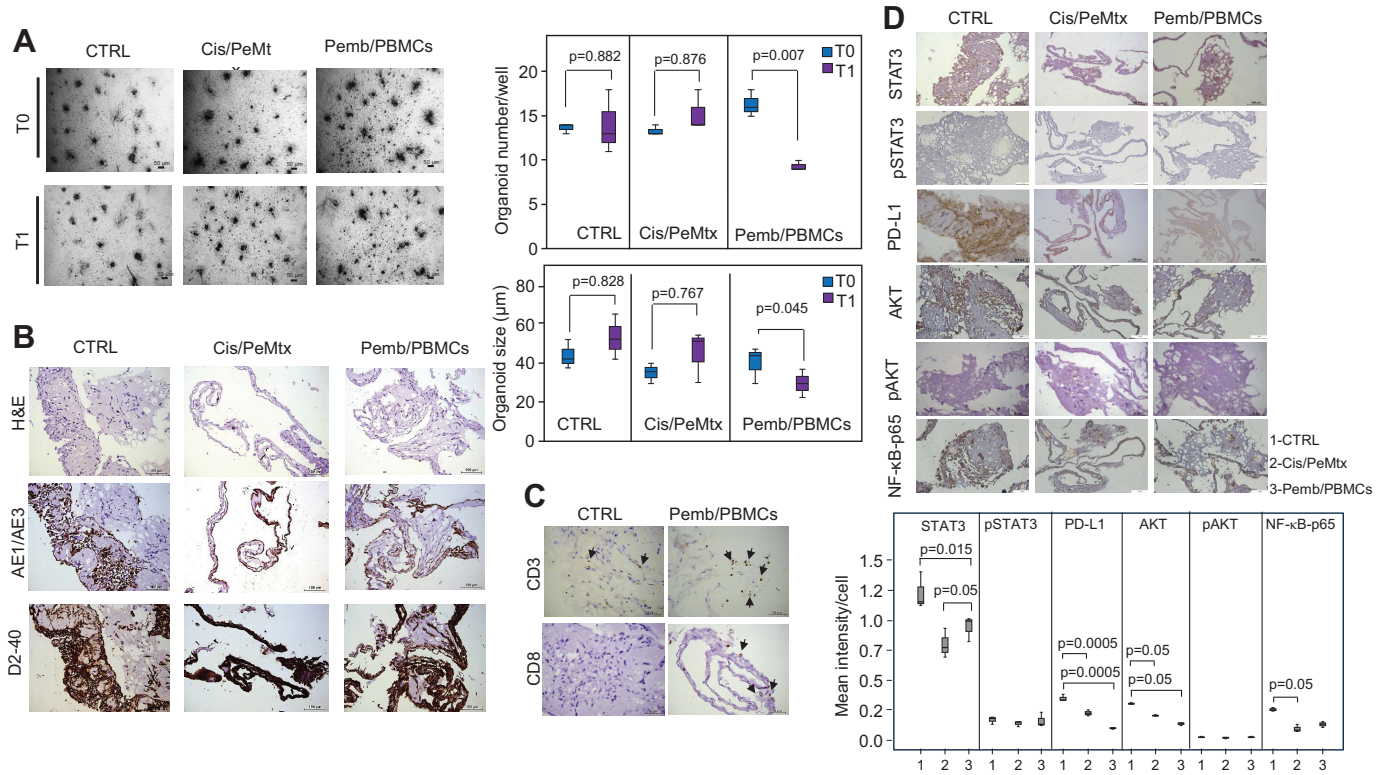

Figure 8. Drug response in BPM-PDOs. Female BPM-PDOs (PM-6) were treated with Cis/PeMtx (30 μM each) or with pembrolizumab (10 μg/mL) in coculture with PBMCs (10^5) from the same patient (Pemb/PBMCs); two cycles of treatments with 3 days between cycles were applied. *A*: representative bright-field microscopy images (scale bar, 50 μm). Organoid growth was quantified by number and size (*right*). *B*: FFPE tumor sections were inspected for H&E and IHC staining of epithelial-related antigen (AE1/AE3) and podoplanin (D2-40). Scale bar, 100 μm. *C*: FFPE tumor sections were inspected for immunohistochemical staining of CD3 and CD8 antigen. Scale bar, 50 μm. *D*: evaluation of the PD-L1 and the STAT3/AKT/NF-κB pathway. Scale bar, 50 μm and 100 μm. Images for control and treatment groups in microscopy experiments were collected at the same time under the same conditions. Data shown are means ± SD of three independent experiments. Comparisons between before (T0) and after (T1) treatments and among groups were evaluated by *t* test analysis and by one-way ANOVA with Tukey's post-hoc analysis, respectively. Cis/PeMtx, cisplatin/pemetrexed; BPM-PDOs, biphasic patient-derived organoids; FFPE, formalin-fixed, paraffin-embedded; H&E, hematoxylin and eosin; IHC, immunohistochemical; PBMCs, peripheral blood mononuclear cells; Pemb, pembrolizumab; PM, pleural mesothelioma.

responded to immunotherapy independently of the presence of tumor-associated macrophages, suggesting that the histotype mainly influences the response to immunotherapy.

Our work supports the growing evidence that PDOs represent a reliable predictive model to test therapeutic responses, especially for immunotherapy. The PM-PDO response in vitro was in line with the patients' clinical response as retrospectively evaluated. In line with our findings, Hocking et al. (30) demonstrated that mesothelioma PDOs established from pleural effusions could be used to test therapeutic sensitivity to cisplatin, accurately reflecting patient-specific responses. Similarly, Cioce et al. (31) showed that PDOs respond heterogeneously to cisplatin and pemetrexed, further validating their role as personalized models for predicting therapeutic outcomes. This suggests PDOs as a promising tool for precision oncology, allowing to guide tailored treatment approaches.

The identification of $CD68^+$ and $CD163^+$ macrophages in PDOs suggests that the tumor microenvironment plays a critical role in the response to therapy, as supported by Cioce et al. (31). Their study showed that mesothelioma-associated fibroblasts may modulate chemotherapy resistance in PDOs via IL-6 secretion, highlighting the importance of noncancerous cells like fibroblasts and macrophages in tumor dynamics (31).

Nevertheless, our findings differ from that of Hocking et al., who recently reported absence of macrophages in PDOs from malignant pleural effusion (30). However, consistently with our results, $CD68^+/CD163^+$ macrophages are considered to promote tumor growth and metastasis (23, 24) and are thought to play a central role in asbestos-induced carcinogenesis and PM formation (25–27). Furthermore, Pezzuto et al. (38) reported that PM is characterized by high percentage of $CD163^+$ cells and by low expression of PD-L1 and CD4, which correlated with lower sensitivity to ICIs. Moreover, ever-growing evidence indicates $CD68^+/CD163^+$ macrophages as a key factor in mediating PD-1/PD-L1 immunosuppression (23). This complements the role of tumor-associated macrophages in modulating immune responses and therapy effectiveness, and it is coherent with the differential response to the immunotherapy that we have observed in EPM-PDOs and BPM-PDOs or SPM-PDOs.

Strengths and Weaknesses

Our study has several strengths. First, the identification of macrophage populations ($CD68^+$ and $CD163^+$) within the PDOs highlights the incorporation of key immune cells, mimicking the tumor microenvironment. This makes the PDO model more reflective of in vivo conditions, allowing

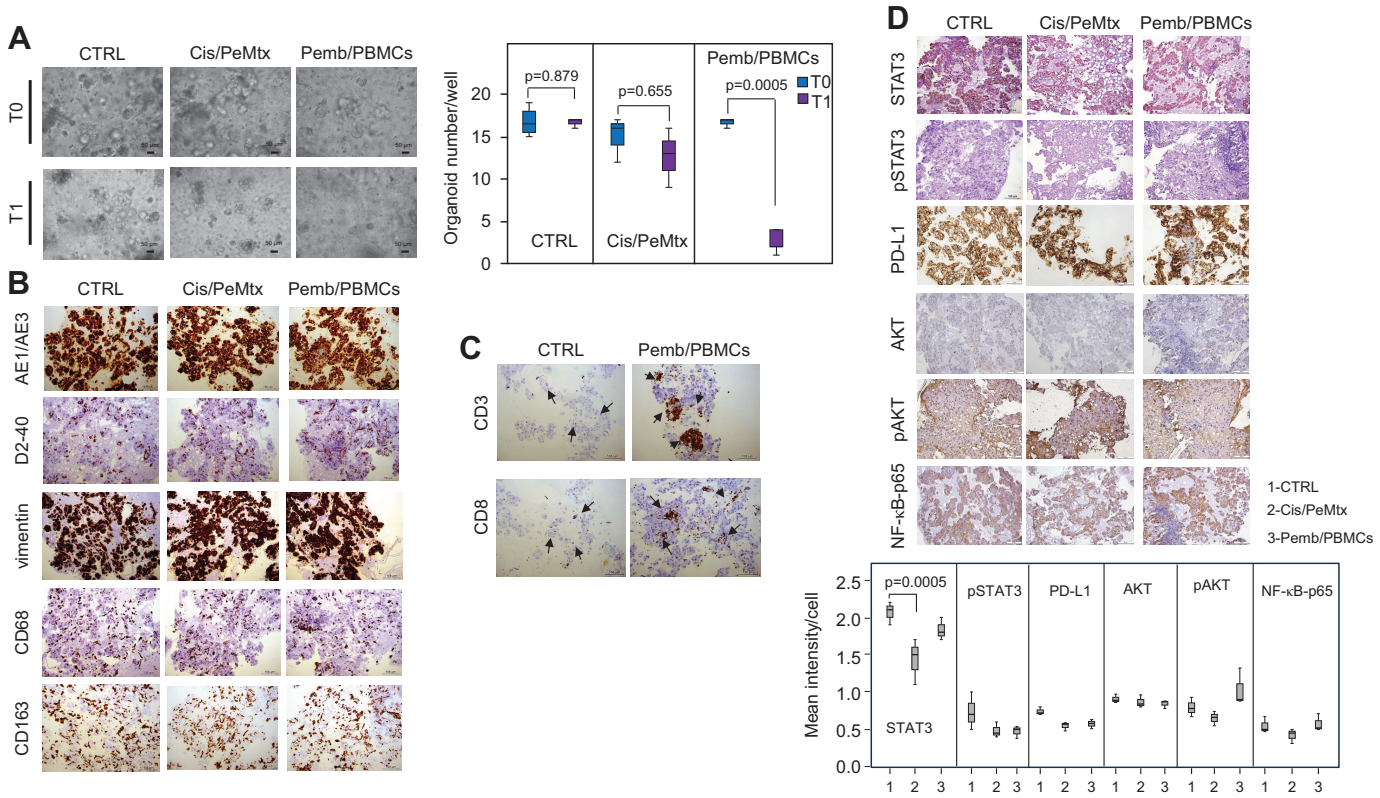

Figure 9. Drug response in SPM-PDOs. Male SPM-PDOs (PM-15) were treated with Cis/PeMtx (30 μM each) or with pembrolizumab (10 μg/mL) in coculture with PBMCs (10^5) from the same patient (Pemb/PBMCs); two cycles of treatments with 3 days between cycles were applied. *A*: representative bright-field microscopy images (scale bar, 50 μm). Organoid growth was quantified by number (*right*). *B*: FFPE tumor sections were inspected for H&E and IHC staining of epithelial-related antigen (AE1/AE3), and podoplanin (D2-40), vimentin, and macrophages (CD68). Scale bar, 100 μm. *C*: FFPE tumor sections were inspected for immunohistochemical staining of CD3 and CD8 antigen. Scale bar, 100 μm. *D*: evaluation of the PD-L1 and the STAT3/AKT/NF-κB pathway. Scale bar, 50 μm and 100 μm. Images for control and treatment groups in microscopy experiments were collected at the same time under the same conditions. Data shown are means ± SD of three independent experiments. Comparisons between before (T0) and after (T1) treatments and among groups were evaluated by *t* test analysis and by 1-way ANOVA with Tukey's post hoc analysis, respectively. Cis/PeMtx, cisplatin/pemetrexed; SPM-PDOs, sarcomatoid patient-derived organoids; FFPE, formalin-fixed, paraffin-embedded; H&E, hematoxylin and eosin; IHC, immunohistochemical; PBMCs, peripheral blood mononuclear cells; Pemb, pembrolizumab; PM, pleural mesothelioma.

for more accurate testing of therapy response. Second, to our knowledge, our study is the first demonstrating the PDOs utility in evaluating the efficacy of immunotherapy, also providing insights into mechanisms of resistance, such as PD-L1 upregulation and STAT3/NF-κB activation. Finally, we confirmed the use of pleural fluid as a reliable and minimally invasive source for generating PDOs, which might be a significant advantage in defining therapeutic strategy, especially for patients who cannot undergo invasive biopsy procedures. This potentially expands the applicability of PDOs in clinical settings.

Weaknesses of the study are mainly related to the procedure of PDO generation and drug screening technique, which is not completely standardized. Second, although the stromal microenvironment is preserved, some anatomical structures, potentially involved in pathobiology mechanisms as nerves and blood vessels, are not represented within PDOs. Furthermore, we did observe a lack of some components of immunological cells, and we are not certain about whether lymphocytes in the parental biopsies were recapitulated in PDOs. However, the presence of T cell in the PDO stroma further supports the response to Pemb, as it is a PD-1 blocker.

Third, the comparative analysis of malignancy with inflammatory plural disease is a little limited given the imbalance between PM-PDOs ($n = 8$) and RM-PDO ($n = 3$).

Moreover, we analyzed the response to chemoimmunotherapy using an optical assessment and a semiquantitative technique, which is not fully reproducible. Finally, the small sample size might have hampered the detection of significant differences among sources of PDOs and histological subtypes in terms of proportion of successful PDO cultures generation.

Conclusions

In conclusion, our study suggests that PF might be an effective and minimally invasive source for generating PDOs both in PM and in patients with NSP, especially those who are unable to undergo surgical procedures. These PDOs accurately preserve the histological and immunohistochemical features of the parental tumors. $CD68^+$ and $CD163^+$ macrophages were found to be crucial components of the PDO microenvironment and may influence the response to therapy. In addition, PDOs offer a promising model for predicting therapeutic responses, making them valuable tools for personalized treatment strategies in mesothelioma.

ETHICAL APPROVALS

The study adhered to the guidelines outlined in the Helsinki Declaration, and samples were processed according to the approval. The study was approved with a waiver of informed consent by the Territorial Ethical Committee of Marche, No. 2023-396, Italy.

DATA AVAILABILITY

All data generated or analyzed during this study are included in this article (and its Supplemental information files) and further data relevant to this study are available by request from the authors.

SUPPLEMENTAL MATERIAL

Supplemental Table S1: https://doi.org/10.5281/zenodo.17076027.
Supplemental Table S2: https://doi.org/10.5281/zenodo.17076043.
Supplemental Table S3: https://doi.org/10.5281/zenodo.17076048.
Supplemental Fig. S1: https://doi.org/10.5281/zenodo.17075999.
Supplemental Fig. S2: https://doi.org/10.5281/zenodo.17076002.
Supplemental Fig. S3: https://doi.org/10.5281/zenodo.17076011.
Supplemental Fig. S4: https://doi.org/10.5281/zenodo.17076017.

GRANTS

This work was supported by the European Union's NextGenerationEU initiative under the Italian Ministry for University and Research—PNRR-PE19—M4C2-I1.3 HEAL ITALIA-2022-2026.

DISCLAIMERS

The funders had no role in data collection, data analysis, data interpretation, or writing of the report.

DISCLOSURES

No conflicts of interest, financial or otherwise, are declared by the authors.

AUTHOR CONTRIBUTIONS

L.V. and F. Monaco conceived and designed research; L.V., F. Monaco, E.J.H., R.F., S.M., O.S., M.M., E.M.B., F.B., and G.G. performed experiments; L.V., F. Monaco, E.C., E.J.H., S.M., O.S., M.M., E.M.B., F.G., F.B., and G.G. analyzed data; M.M., E.M.B., J.N., and F. Monaco interpreted results of experiments; L.V. and F. Monaco prepared figures; F.G. drafted manuscript; G. Moroncini, A.P., and F.G. edited and revised manuscript; L.V., F. Monaco, E.C., E.J.H., R.F., S.M., O.S., G. Moroncini, A.P., F.G., F.B., G.G., L.Z., M.B., G. Matullo, J.N., L.S., N.R., K.B., M.T., and F. Mei approved final version of manuscript.

REFERENCES

1. **Chimed-Ochir O**, **Arachi D**, **Driscoll T**, **Lin RT**, **Takala J**, **Takahashi K.** Burden of mesothelioma deaths by national income category: current status and future implications. *Int J Environ Res Public Health* 17: 6900, 2020. doi:10.3390/ijerph17186900.
2. **Hodgson JT**, **McElvenny DM**, **Darnton AJ**, **Price MJ**, **Peto J.** The expected burden of mesothelioma mortality in Great Britain from 2002 to 2050. *Br J Cancer* 92: 587–593, 2005. doi:10.1038/sj.bjc.6602307.
3. **Huang J**, **Chan SC**, **Pang WS**, **Chow SH**, **Lok V**, **Zhang L**, **Lin X**, **Lucero-Prisno DE**, **Xu W**, **Zheng ZJ**, **Elcarte E**, **Withers M**, **Wong MCS**; **NCD Global Health Research Group, Association of Pacific Rim Universities (APRU).** Global incidence, risk factors, and temporal trends of mesothelioma: a population-based study. *J Thorac Oncol* 18: 792–802, 2023. doi:10.1016/j.jtho.2023.01.095.
4. **Marinaccio A**, **Binazzi A**, **Cauzillo G**, **Cavone D**, **Zotti RD**, **Ferrante P**, **Gennaro V**, **Gorini G**, **Menegozzo M**, **Mensi C**, **Merler E**, **Mirabelli D**, **Montanaro F**, **Musti M**, **Pannelli F**, **Romanelli A**, **Scarselli A**, **Tumino R**; **Italian Mesothelioma Register (ReNaM) Working Group.** Analysis of latency time and its determinants in asbestos related malignant mesothelioma cases of the Italian register. *Eur J Cancer* 43: 2722–2728, 2007. doi:10.1016/j.ejca.2007.09.018.
5. **Han J**, **Park S**, **Yon DK**, **Lee SW**, **Woo W**, **Dragioti E**, **Koyanagi A**, **Jacob L**, **Kostev K**, **Radua J**, **Lee S**, **Shin JI**, **Smith L.** Global, regional, and national burden of mesothelioma 1990-2019: a systematic analysis of the global burden of disease study 2019. *Ann Am Thorac Soc* 20: 976–983, 2023. doi:10.1513/AnnalsATS.202209-802OC.
6. **Frank AL.** Global use of asbestos - legitimate and illegitimate issues. *J Occup Med Toxicol* 15: 16, 2020. doi:10.1186/s12995-020-00267-y.
7. **Zhao Z**, **Li J**, **Tan F**, **Xue Q**, **Gao S**, **He J.** Assessing the global burden of mesothelioma: trends, socioeconomic influences, and asbestos exposure - a retrospective cohort study. *Int J Surg* 111: 93–103, 2025. doi:10.1097/JS9.0000000000001900.
8. **Yoshida M**, **Jimbo N**, **Tsukamoto R**, **Itoh T**, **Kawahara K**, **Mitsui S**, **Tanaka Y**, **Maniwa Y.** Sarcomatoid mesothelioma diagnosed in a patient with mesothelioma in situ: a case report on morphologic differences after 9-month interval with details analysis of cytology in early-stage mesothelioma. *Diagn Pathol* 18: 126, 2023. doi:10.1186/s13000-023-01416-7.
9. **Sundaralingam A**, **Aujayeb A**, **Jackson KA**, **Pellas EI**, **Khan II**, **Chohan MT**, **Joosten R**, **Boersma A**, **Kerkhoff J**, **Bielsa S**, **Porcel JM**, **Rozman A**, **Marc-Malovrh M**, **Welch H**, **Symonds J**, **Anevlavis S**, **Froudrakis M**, **Mei F**, **Zuccatosta L**, **Gasparini S**, **Gonnelli F**, **Dhaliwal I**, **Mitchell MA**, **Fjaellegaard K**, **Petersen JK**, **Ellayeh M**, **Rahman NM**, **Burden T**, **Bodtger U**, **Koegelenberg CFN**, **Maskell NA**, **Janssen J**, **Bhatnagar R.** Investigation and outcomes in patients with nonspecific pleuritis: results from the International Collaborative Effusion database. *ERJ Open Res* 9: 00599-02022, 2023. doi:10.1183/23120541.00599-2022.
10. **Bou-Samra P**, **Chang A**, **Azari F**, **Kennedy G**, **Segil A**, **Guo E**, **Marmarelis M**, **Langer C**, **Singhal S.** Epidemiological, therapeutic, and survival trends in malignant pleural mesothelioma: a review of the National Cancer Database. *Cancer Med* 12: 12208–12220, 2023. doi:10.1002/cam4.5915.
11. **Carbone M**, **Yang H**, **Pass HI**, **Taioli E.** Did the ban on asbestos reduce the incidence of mesothelioma? *J Thorac Oncol* 18: 694–697, 2023. doi:10.1016/j.jtho.2023.03.013.
12. **Gao Y**, **Kruithof-de Julio M**, **Peng RW**, **Dorn P.** Organoids as a model for precision medicine in malignant pleural mesothelioma: where are we today? *Cancers (Basel)* 14: 3758, 2022. doi:10.3390/cancers14153758.
13. **Nel AE**, **Pavlisko EN**, **Roggli VL.** The interplay between the immune system, tumor suppressor genes, and immune senescence in mesothelioma development and response to immunotherapy. *J Thorac Oncol* 19: 551–564, 2024. doi:10.1016/j.jtho.2023.11.017.
14. **Fennell DA**, **Ewings S**, **Ottensmeier C**, **Califano R**, **Hanna GG**, **Hill K**, **Danson S**, **Steele N**, **Nye M**, **Johnson L**, **Lord J**, **Middleton C**, **Szlosarek P**, **Chan S**, **Gaba A**, **Darlison L**, **Wells-Jordan P**, **Richards C**, **Poile C**, **Lester JF**, **Griffiths G**; **CONFIRM trial investigators.** Nivolumab versus placebo in patients with relapsed malignant mesothelioma (CONFIRM): a multicentre, double-blind, randomised, phase 3 trial. *Lancet Oncol* 22: 1530–1540, 2021 [Erratum in *Lancet Oncol* 26: e238, 2025]. doi:10.1016/S1470-2045(21)00471-X.
15. **Scherpereel A**, **Mazieres J**, **Greillier L**, **Lantuejoul S**, **Do P**, **Bylicki O**, **Monnet I**, **Corre R**, **Audigier-Valette C**, **Locatelli-Sanchez M**, **Molinier O**, **Guisier F**, **Urban T**, **Ligeza-Poisson C**, **Planchard D**, **Amour E**, **Morin F**, **Moro-Sibilot D**, **Zalcman G**; **French Cooperative Thoracic Intergroup.** Nivolumab or nivolumab plus ipilimumab in patients with relapsed malignant pleural mesothelioma (IFCT-1501 MAPS2): a multicentre, open-label, randomised, non-comparative, phase 2 trial. *Lancet Oncol* 20: 239–253, 2019 [Erratum in *Lancet Oncol* 20: e132, 2019]. doi:10.1016/S1470-2045(18)30765-4.
16. **Gray SG**, **Meirson T**, **Mutti L.** Based on the real-world results from australia, immunotherapy is not a good option for patients with mesothelioma. *J Thorac Oncol* 19: 541–546, 2024. doi:10.1016/j.jtho.2024.01.016.

17. **Lievense LA**, **Cornelissen R**, **Bezemer K**, **Kaijen-Lambers ME**, **Hegmans JP**, **Aerts JG.** Pleural effusion of patients with malignant mesothelioma induces macrophage-mediated T cell suppression. *J Thorac Oncol* 11: 1755–1764, 2016. doi:10.1016/j.jtho.2016.06.021.
18. **Muruganandan S**, **Duong V.** Malignant pleural effusion in malignant pleural mesothelioma: an innocent bystander? *Chest* 160: 1602–1603, 2021. doi:10.1016/j.chest.2021.06.074.
19. **Salaroglio IC**, **Kopecka J**, **Napoli F**, **Pradotto M**, **Maletta F**, **Costardi L**, **Gagliasso M**, **Milosevic V**, **Ananthanarayanan P**, **Bironzo P**, **Tabbò F**, **Cartia CF**, **Passone E**, **Comunanza V**, **Ardissone F**, **Ruffini E**, **Bussolino F**, **Righi L**, **Novello S**, **Di Maio M**, **Papotti M**, **Scagliotti GV**, **Riganti C.** Potential diagnostic and prognostic role of microenvironment in malignant pleural mesothelioma. *J Thorac Oncol* 14: 1458–1471, 2019 [Erratum in *J Thorac Oncol* 14: 2023, 2019]. doi:10.1016/j.jtho.2019.03.029.
20. **Vazquez-Armendariz AI**, **Tata PR.** Recent advances in lung organoid development and applications in disease modeling. *J Clin Invest* 133: e170500, 2023. doi:10.1172/JCI170500.
21. **Mazzocchi A**, **Devarasetty M**, **Herberg S**, **Petty WJ**, **Marini F**, **Miller L**, **Kucera G**, **Dukes DK**, **Ruiz J**, **Skardal A**, **Soker S.** Pleural effusion aspirate for use in 3D lung cancer modeling and chemotherapy screening. *ACS Biomater Sci Eng* 5: 1937–1943, 2019. doi:10.1021/acsbiomaterials.8b01356.
22. **Choi W**, **Kim YH**, **Woo SM**, **Yu Y**, **Lee MR**, **Lee WJ**, **Chun JW**, **Sim SH**, **Chae H**, **Shim H**, **Lee KS**, **Kong SY.** Establishment of patient-derived organoids using ascitic or pleural fluid from cancer patients. *Cancer Res Treat* 55: 1077–1086, 2023. doi:10.4143/crt.2022.1630.
23. **Kim M**, **Mun H**, **Sung CO**, **Ho EJ**, **Jeon HJ**, **Chun SM**, **Jung DJ**, **Shin TH**, **Jeong GS**, **Kim DK**, **Choi EK**, **Jeong SY**, **Taylor AM**, **Jain S**, **Meyerson M**, **Jang SJ.** Patient-derived lung cancer organoids as in vitro cancer models for therapeutic screening. *Nat Commun* 10: 3991, 2019. doi:10.1038/s41467-019-11867-6.
24. **Patro R**, **Duggal G**, **Love MI**, **Irizarry RA**, **Kingsford C.** Salmon provides fast and bias-aware quantification of transcript expression. *Nat Methods* 14: 417–419, 2017. doi:10.1038/nmeth.4197.
25. **Love MI**, **Huber W**, **Anders S.** Moderated estimation of fold change and dispersion for RNA-seq data with DESeq2. *Genome Biol* 15: 550, 2014. doi:10.1186/s13059-014-0550-8.
26. **Wickham H.** *Ggplot2: Elegant Graphics for Data Analysis* (2nd ed.). Springer, 2016.
27. **Scherpereel A**, **Opitz I**, **Berghmans T**, **Psallidas I**, **Glatzer M**, **Rigau D**, **Astoul P**, **Bölükbas S**, **Boyd J**, **Coolen J**, **De Bondt C**, **De Ruysscher D**, **Durieux V**, **Faivre-Finn C**, **Fennell D**, **Galateau-Salle F**, **Greillier L**, **Hoda MA**, **Klepetko W**, **Lacourt A**, **McElnay P**, **Maskell NA**, **Mutti L**, **Pairon J-C**, **Van Schil P**, **Van Meerbeeck JP**, **Waller D**, **Weder W**, **Cardillo G**, **Putora PM.** ERS/ESTS/EACTS/ESTRO guidelines for the management of malignant pleural mesothelioma. *Eur Respir J* 55: 1900953, 2020. doi:10.1183/13993003.00953-2019.
28. **Carbone M**, **Minaai M**, **Takinishi Y**, **Pagano I**, **Yang HJ.** Preventive and therapeutic opportunities: targeting BAP1 and/or HMGB1 pathways to diminish the burden of mesothelioma. *J Transl Med* 21: 749, 2023. doi:10.1186/s12967-023-04614-5.
29. **Zahiu T**, **Mihu CM**, **Bosca BA**, **Mărginean M**, **Mocan LP**, **Stefan RA**, **Sufleţel RT**, **Mihu C**, **Melincovici CS.** Molecular insights into pleural mesothelioma: unveiling pathogenic mechanisms and therapeutic opportunities. *Diagnostics (Basel)* 15: 1323, 2025. doi:10.3390/diagnostics15111323.
30. **Hocking AJ**, **Mortimer LA**, **Farrall AL**, **Russell PA**, **Klebe S.** Establishing mesothelioma patient-derived organoid models from malignant pleural effusions. *Lung Cancer* 191: 107542, 2024. doi:10.1016/j.lungcan.2024.107542.
31. **Cioce M**, **Gatti V**, **Napolitano F**, **Giorgiano NM**, **Marra A**, **Portella G**, **Fiorelli A**, **Pentimalli F**, **Fazio VM.** Mesothelioma-associated fibroblasts modulate the response of mesothelioma patient-derived organoids to chemotherapy via interleukin-6. *Int J Mol Sci* 25: 5355, 2024. doi:10.3390/ijms25105355.
32. **Walz S**, **Pollehne P**, **Vollmer P**, **Aicher WK**, **Stenzl A**, **Harland N**, **Amend B.** Effects of scaffolds on urine- and urothelial carcinoma tissue-derived organoids from bladder cancer patients. *Cells* 12: 2108, 2023. doi:10.3390/cells12162108.
33. **Ito F**, **Kato K**, **Yanatori I**, **Maeda Y**, **Murohara T**, **Toyokuni S.** Matrigel-based organoid culture of malignant mesothelioma reproduces cisplatin sensitivity through CTR1. *BMC Cancer* 23: 487, 2023. doi:10.1186/s12885-023-10966-4.
34. **Sato Y**, **Elbadawy M**, **Suzuki K**, **Tsunedomi R**, **Nagano H**, **Ishihara Y**, **Yamamoto H**, **Azakami D**, **Uchide T**, **Nabeta R**, **Fukushima R**, **Abugomaa A**, **Kaneda M**, **Yamawaki H**, **Shinohara Y**, **Usui T**, **Sasaki K.** Establishment of an experimental model of canine malignant mesothelioma organoid culture using a three-dimensional culture method. *Biomed Pharmacother* 162: 114651, 2023. doi:10.1016/j.biopha.2023.114651.
35. **de Visser KE**, **Joyce JA.** The evolving tumor microenvironment: from cancer initiation to metastatic outgrowth. *Cancer Cell* 41: 374–403, 2023. doi:10.1016/j.ccell.2023.02.016.
36. **Yao N**, **Jing N**, **Lin J**, **Niu W**, **Yan W**, **Yuan H**, **Xiong Z**, **Hou Q**, **Qiao X**, **Liu Q**, **Cao J**, **Li N.** Patient-derived tumor organoids for cancer immunotherapy: culture techniques and clinical application. *Invest New Drugs* 43: 394–404, 2025. doi:10.1007/s10637-025-01523-w.
37. **Cattaneo CM**, **Dijkstra KK**, **Fanchi LF**, **Kelderman S**, **Kaing S**, **van Rooij N**, **van den Brink S**, **Schumacher TN**, **Voest EE.** Tumor organoid-T-cell coculture systems. *Nat Protoc* 15: 15–39, 2020. doi:10.1038/s41596-019-0232-9.
38. **Pezzuto F**, **Lunardi F**, **Vedovelli L**, **Fortarezza F**, **Urso L**, **Grosso F**, **Ceresoli GL**, **Kern I**, **Vlacic G**, **Faccioli E**, **Schiavon M**, **Gregori D**, **Rea F**, **Pasello G**, **Calabrese F.** P14/ARF-positive malignant pleural mesothelioma: a phenotype with distinct immune microenvironment. *Front Oncol* 11: 653497, 2021. doi:10.3389/fonc.2021.653497.